

Strength and fatigue fracture behavior of Al–Zn–Mg–Cu–Zr(–Sn) alloys

Lu CHEN¹, An YAN¹, Hua-shan LIU¹, Xiao-qian LI²

1. School of Materials Science and Engineering, Central South University, Changsha 410083, China;

2. School of Mechanical and Electric Engineering, Central South University, Changsha 410083, China

Received 12 September 2012; accepted 14 January 2013

Abstract: The strength and fatigue fracture behavior of Al–Zn–Mg–Cu–Zr(–Sn) alloys were studied by performing tensile tests and fatigue crack propagation (FCP) tests. The microstructures of the experimental alloys were further analyzed using optical microscopy (OM), scanning electron microscopy (SEM), and transmission electron microscopy (TEM); phase analysis of these alloys was conducted with an X-ray diffraction (XRD). The results show that when Sn is included, growth of the recrystallization grains in the solution-treated Al–Zn–Mg–Cu–Zr alloy is obstructed, the precipitation-free zone (PFZ) of the overaged Al–Zn–Mg–Cu–Zr–Sn alloy becomes narrow, and the grain boundary precipitates are smaller. Consequently, the FCP resistance is higher. In addition, the overaged Sn-containing alloy has considerably higher tensile strength than the alloy without Sn.

Key words: Al–Zn–Mg–Cu–Zr; Sn; strength; fatigue fracture behavior; microstructure

1 Introduction

7xxx-series Al–Zn–Mg–Cu alloys have many attractive properties, including low density, high strength, and high specific strength and stiffness. Thus, they are widely applied to the aerospace industry as some of the most important structural materials. Before the 1960s, peak-aging treatment was used for this series of alloys in order to maximize their strength. However, the precipitates at the grain boundaries after peak-aging treatment tend to form a continuous chain, resulting in high susceptibility to stress corrosion cracking (SCC) and relatively low fatigue crack growth resistance. As primary structural materials in the aircraft industry, 7xxx-series alloys must have high strength and fatigue resistance in order to withstand repeated cyclic loading [1,2].

To improve the strength, SCC resistance, and fatigue crack growth resistance of the 7xxx-series alloys, various heat treatments such as T76, T736 (T74), T7351, and retrogression and reaging (RRA) have been extensively studied and developed. Trace elements are also often added to the alloys to improve their strength.

It is well known that the microstructure and properties of aluminum alloys are strongly affected by

the addition of trace elements. For example, the addition of Zr can improve the mechanical properties of 7xxx-series alloys through the formation of Al₃Zr, which is coherent with the matrix and can prevent recrystallization [3]. In recent years, considerable attention has also been focused on the addition of rare-earth (RE) elements. BAI et al [4] revealed that the resistance of Al–Cu–Mg–Ag alloys to fatigue crack propagation (FCP) can be significantly enhanced by the addition of Er. ZHANG et al [5] investigated the addition of Yb and reported that this element can improve the ultimate strength and fracture toughness of Al–Zn–Mg–Cu–Zr alloys.

Because RE elements are expensive, researchers have turned their attention to another less-expensive element, Sn. Trace addition of Sn has been reported to suppress low-temperature aging, but it also obviously enhances age-hardening effects at elevated temperatures for several Al–Cu alloys [6–8]. BANERJEE et al [9] concluded that the addition of Sn improves the tensile strength and toughness of Al–Cu–Mg alloys. MOHAMED et al [10] revealed that the addition of 0.05% Sn (mass fraction) improved the mechanical properties of cast Al–Si–Mg alloys. In view of these beneficial effects of Sn addition on Al–Cu-based and Al–Si–Mg alloys, it may be possible to develop a

cost-effective Al–Zn–Mg–Cu–Sn alloy with superior overall performance. However, there are no reports on the addition of Sn to 7xxx-series alloys. The purpose of this research, therefore, was to study the effect of Sn on the strength and fatigue fracture behavior of Al–Zn–Mg–Cu–Zr alloys.

2 Experimental

The actual compositions of the investigated alloys are listed in Table 1. The starting materials included pure bulk Al (99.99%), Mg (99.9%), Zn (99.9%), and Sn (99.9%) as well as Al–52%Cu and Al–4.3%Zr master alloys.

The alloys used in this study were prepared as follows. Appropriate amounts of the starting materials were melted and refined in an electric resistance furnace at 750–780 °C and then cast into rectangular ingots with dimensions of 270 mm×135 mm×32 mm. The cast ingots of the Al–Zn–Mg–Cu–Zr–(Sn) alloys were allowed to homogenize, after which they were air-cooled to room temperature and then scalped and hot-rolled at about 420 °C into 11 mm-thick plates. The specimens were cut from the rolled-plate samples, solution-treated in a salt bath at 470 °C for 90 min, and then water-quenched to room temperature. Finally, the samples were double-aged at 120 °C for 24 h and at 175 °C for 10 h.

Five specimens for each alloy were prepared so that the tensile tests could measure the properties along the longitudinal direction of the rolled plates. The tensile properties of the alloys were measured at a constant speed of 2 mm/min using an Instron 4505 test machine.

To study the FCP behavior of the alloys, 9.6 mm-thick compact-tension (CT) fracture mechanics specimens with a width of 50 mm oriented in the transverse–longitudinal (T–L) direction (the crack plane and the crack propagation direction are parallel to the T–L plane) were machined according to ASTM standard E 647 [11]. The dimensions of the fatigue specimens are shown in Fig. 1. The stress-intensity factor range (ΔK) for the CT specimens was calculated using Eq. (1):

$$\Delta K = \frac{\Delta P}{B\sqrt{W}} \frac{2+\alpha}{(1-\alpha)^{3/2}} (0.886 + 4.64\alpha - 13.32\alpha^2 + 14.72\alpha^3 - 5.6\alpha^4) \quad (1)$$

where ΔP is the applied load amplitude; B is the

specimen thickness; W is the specimen width; $\alpha=a/W$ and a is the crack length. All FCP tests were conducted at a stress ratio ($R=K_{\min}/K_{\max}$) of 0.1 with a loading frequency of 10 Hz using an MTS 858 fatigue tester at room temperature in the laboratory air environment. The crack length was monitored using the elastic compliance technique.

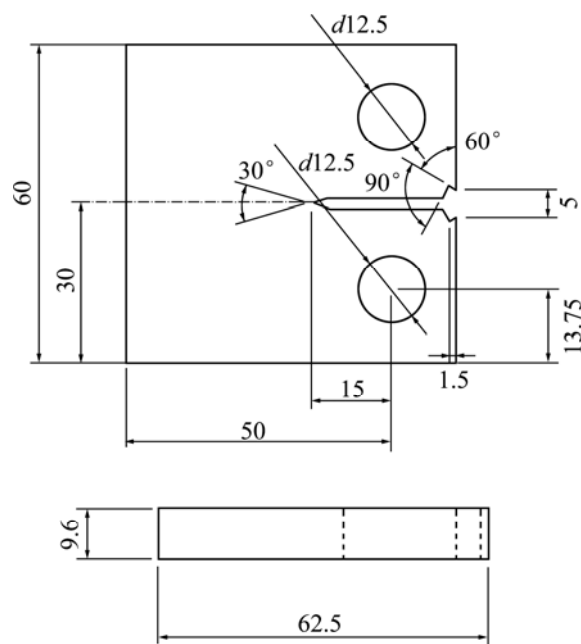


Fig. 1 Dimensional details of fatigue test specimen (CT) (unit: mm)

The microstructures of the samples were examined using OM and SEM (Quanta 200) coupled with energy-dispersive X-ray spectroscopy (EDS, GENESIS 60S). Phase analysis of the alloys was conducted with XRD (Rigaku D/max 2500) at a scanning speed of 2 (°)/min. The fracture surfaces of the samples and the microstructures associated with the fractures were analyzed using SEM and EDS.

TEM was employed to characterize the microstructures of the aged alloys. The specimens for TEM were thin slices (diameter: 3 mm) that were electropolished using twin-jet equipment at a voltage of 10 V in a solution of 70% methanol and 30% nitric acid at approximately –20 °C. Subsequently, the slices were cleaned in ethanol at room temperature for at least 5 min and then examined by a JEM–2100F TEM machine operating at 200 kV.

Table 1 Actual compositions of experimental alloys

Alloy	w(Zn)/%	w(Mg)/%	w(Cu)/%	w(Zr)/%	w(Sn)/%	w(Al)/%
Al–Zn–Mg–Cu–Zr	6.19	2.31	2.23	0.10	0	Bal.
Al–Zn–Mg–Cu–Zr–Sn	6.21	2.29	2.21	0.10	0.21	Bal.

3 Results

3.1 Tensile properties

The tensile properties of the aged alloys are listed in Table 2. It can be seen that the ultimate tensile strength (σ_b) of the Al-Zn-Mg-Cu-Zr alloy increases from 482 MPa to 505 MPa after Sn addition, and the yield strength ($\sigma_{0.2}$) improves from 415 MPa to 432 MPa, while the elongation (δ) shows a slight decrease from 10.8% to 10.5%.

Table 2 Room-temperature tensile properties of aged Al-Zn-Mg-Cu-Zr-(Sn) alloys

Alloy	σ_b /MPa	$\sigma_{0.2}$ /MPa	δ /%
Al-Zn-Mg-Cu-Zr	482±4	415±3	10.8±0.1
Al-Zn-Mg-Cu-Zr-Sn	505±5	432±4	10.5±0.1

3.2 Fatigue crack propagation

The variation in the FCP rate (da/dN) with the stress-intensity factor range (ΔK) is illustrated in Fig. 2 for both aged alloys. Both da/dN — ΔK curves display three typical stages from the threshold range of the stress-intensity factor (ΔK_{th}) up to the critical stress-intensity amplitude at which the final fatigue fracture occurs: 1) a low-speed propagation (near-

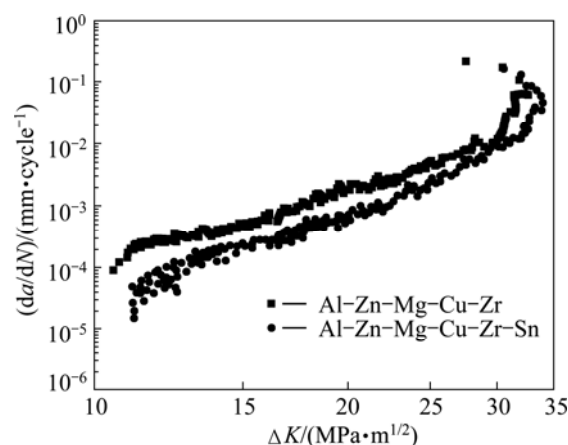


Fig. 2 FCP rate, da/dN , as function of ΔK for aged alloys

threshold) stage, 2) a steady-state crack propagation (Paris) stage, and 3) a high-growth-rate stage. In addition, it is clear that the addition of Sn increases the crack propagation resistance of the Al-Zn-Mg-Cu-Zr alloy during all stages, namely, the Sn-containing alloy shows a lower FCP rate. This phenomenon is further confirmed by the fatigue fracture characteristics, as shown in Figs. 3–5.

Figures 3(a) and (b) show the near-threshold fatigue fracture surfaces of the aged alloys. The corresponding high-magnification observations are shown in Figs. 3(c)

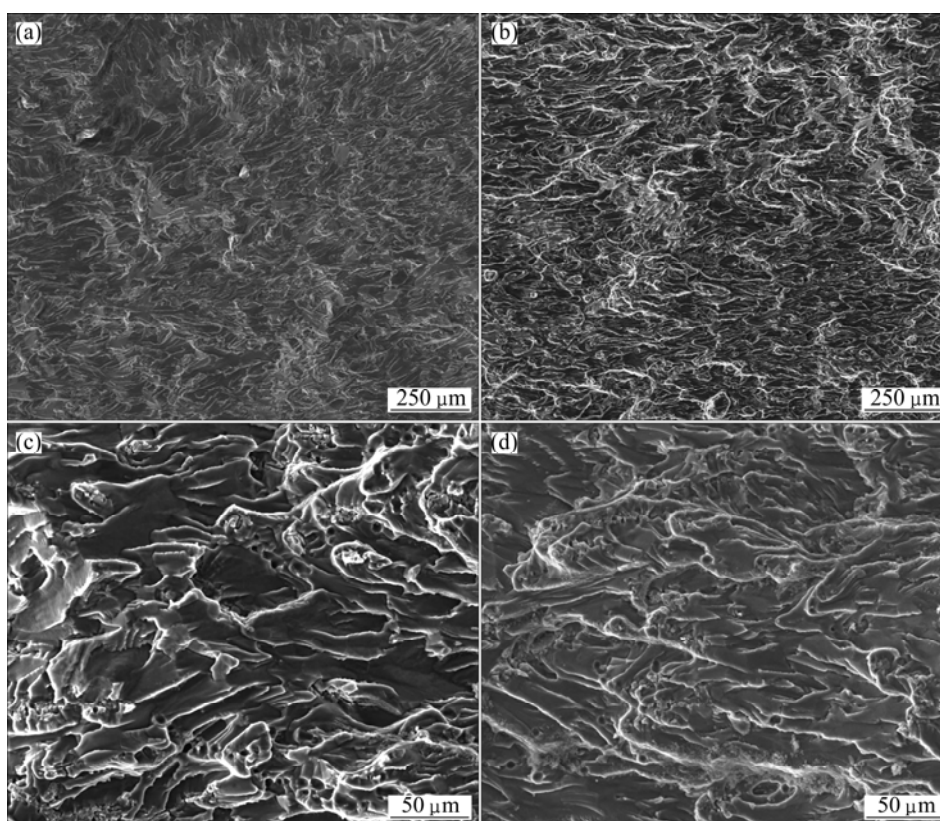


Fig. 3 SEM images of near-threshold fatigue fracture surfaces of aged Al-Zn-Mg-Cu-Zr alloy (a, c) and Al-Zn-Mg-Cu-Zr-Sn alloy (b, d) (crack growth is from left to right)

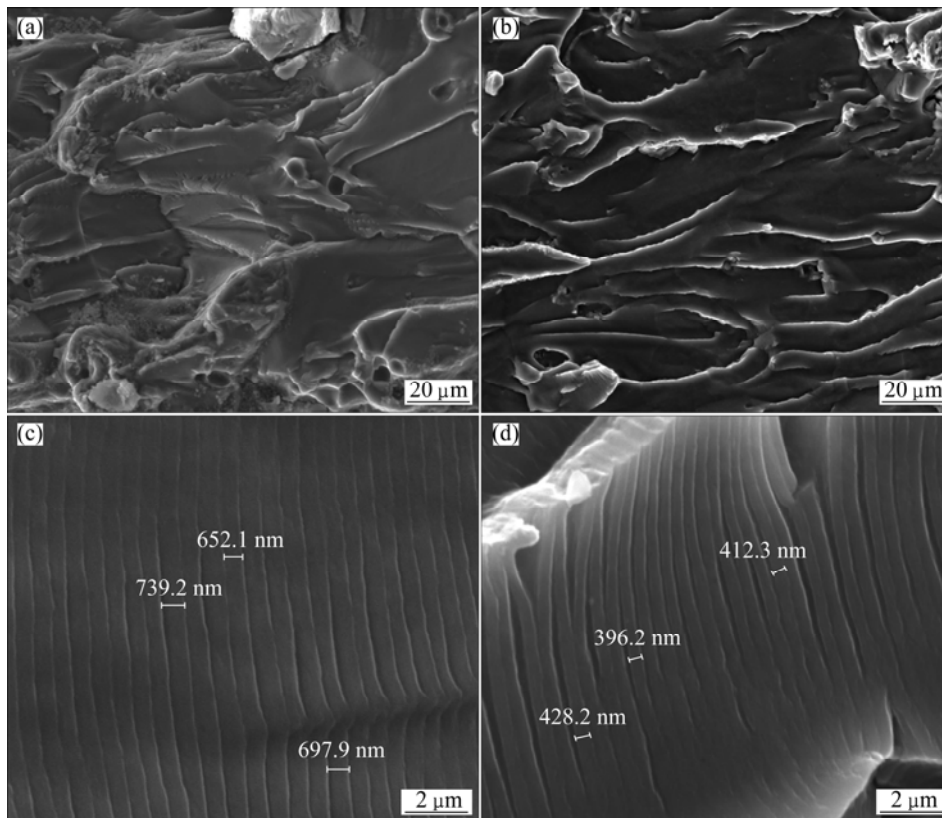


Fig. 4 SEM images of fatigue fracture surfaces in steady-state crack-propagation (Paris) stage for aged Al-Zn-Mg-Cu-Zr alloy (a, c) and Al-Zn-Mg-Cu-Zr-Sn alloy (b, d) (crack growth is from left to right)

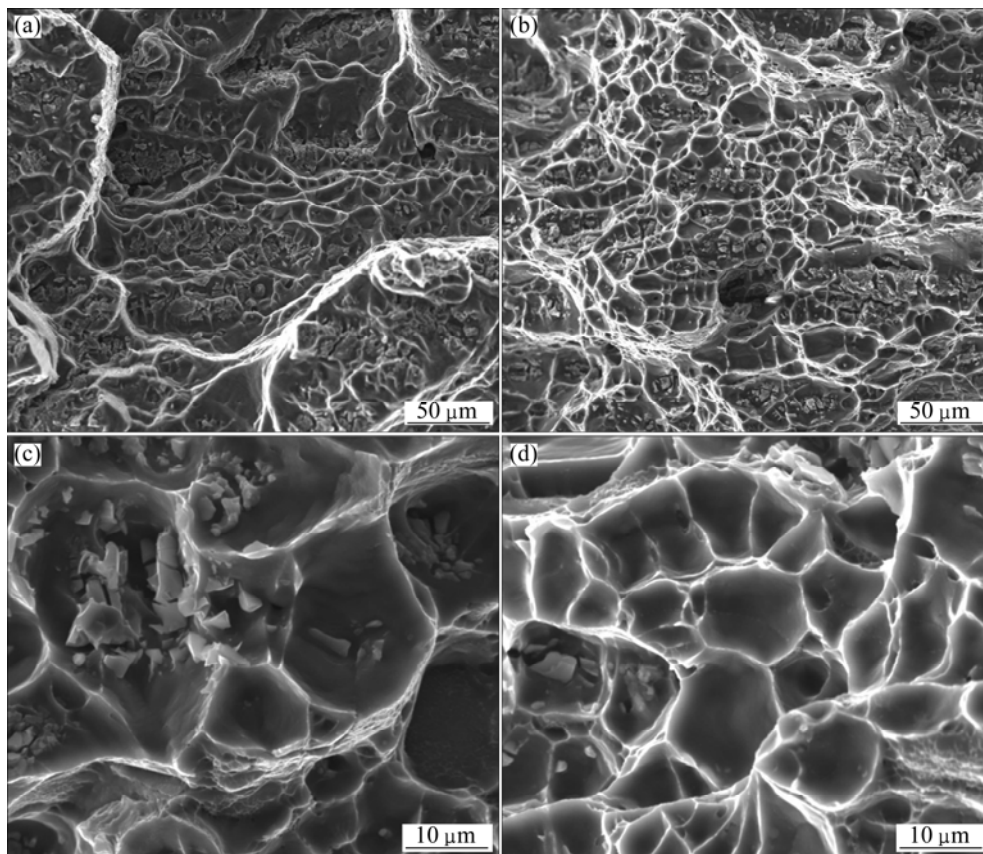


Fig. 5 SEM images of fatigue fracture surfaces of aged Al-Zn-Mg-Cu-Zr alloy (a, c) and Al-Zn-Mg-Cu-Zr-Sn alloy (b, d) in high-growth-rate regime (crack growth is from left to right)

and (d), respectively. These fracture surfaces exhibit microplastic cleavage fracture features and are characterized by fluted failure and transgranular fractures. Many fatigue plateaus joined by tear ridges are also clearly observed. It has been proposed that fluting occurs because of the scarcity of active slip systems and the coalescence of voids [12]. Comparison of Fig. 3(a) with 3(b) and that of Fig. 3(c) with 3(d) show that fluting in the case of the Sn-containing alloy is more slender, which indicates a lower FCP rate in the near-threshold stage (Fig. 2).

SEM images of the fatigue fracture surfaces in the Paris regime are shown in Fig. 4. This region contains pockets of cleavage steps formed during cyclic deformation and microscopic voids formed around dispersoid particles, indicating that the microvoid aggregation mechanism plays an important role in fatigue fracture. It is generally accepted that the voids can be considered equivalent to the second-phase particles having zero stiffness. Therefore, a gradual increase in the size and relative volume fraction of voids occurs during cyclic deformation, which ultimately results in an increase in crack-tip extension [13]. As revealed in Fig. 4(b), after the addition of Sn, the fracture surface seems to be composed of fewer microvoids, which leads to higher FCP resistance [14].

The fatigue striations shown in Figs. 4(c) and (d) are typical fracture characteristics in the Paris stage. Each striation is perpendicular to the crack growth direction and can be regarded as the microscopic trace of one fatigue stress cycle. In other words, the width of the striation reflects the FCP rate to some degree [15]. By comparing Figs. 4(c) and (d), one can also clearly see that the width of the striations is narrower for Al–Zn–Mg–Cu–Zr–Sn than for Al–Zn–Mg–Cu–Zr, implying that the addition of Sn lowers the crack growth rate. This observation is consistent with the results deduced from the FCP curves shown in Fig. 2.

To highlight the differences between the features of the fatigue fractures of these two alloys in the high-growth-rate stage, the morphology of the fatigue fractures is investigated (Fig. 5), which roughly reveals regions of locally ductile failure. The region consists predominantly of a dispersion of dimples; tear ridges are also observed in Figs. 5(c) and (d). After the addition of Sn, pockets of fine shallow dimples formed, and these are distributed randomly throughout the surface, suggesting a lower FCP rate [16].

4 Discussion

The differences in the strength and fatigue fracture behavior of the Al–Zn–Mg–Cu–Zr(–Sn) alloys can be

attributed to the differences in their microstructural features, including their grain sizes, grain boundary structures, precipitates, and additional phases formed during solidification.

Metallographs of the aged alloys used in this study are shown in Fig. 6, which reveal that the microstructures are characterized by equiaxed grains. This indicates that recrystallization occurred in the alloys during solution treatment. Grain size analyses were carried out adopting a linear intercept method. It is shown that the grain size of Al–Zn–Mg–Cu–Zr alloy is about 21 μm (Fig. 6(a)), for the Al–Zn–Mg–Cu–Zr alloy including 0.2%Sn. The grain size is refined with average grain size of about 13 μm (Fig. 6(b)). It is also apparent that the grain size of the aged Al–Zn–Mg–Cu–Zr alloy is refined when Sn is added. This suggests that Sn may act as an obstacle to the growth of recrystallization grains in solution-treated Al–Zn–Mg–Cu–Zr alloy. It is accepted that finer grains will cause an increase in strength, resulting in improved tensile properties [17,18].

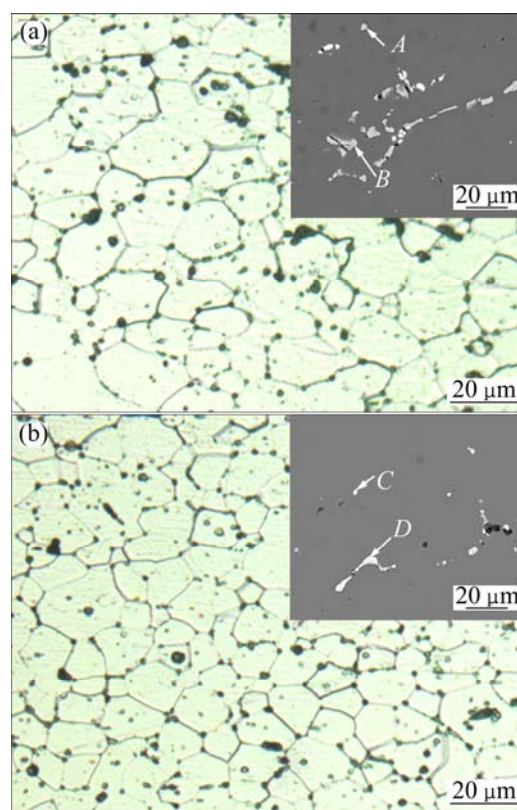


Fig. 6 Metallographs and SEM images of aged Al–Zn–Mg–Cu–Zr alloy (a) and aged Al–Zn–Mg–Cu–Zr–Sn alloy (b)

Grain boundaries are known to be one of the major barriers to fatigue crack growth (especially to short crack growth) in most engineering metallic materials [19–22]. BILBY et al [23] described the crack and the plastic deformation zone in the vicinity of the crack tip as an array of continuously distributed dislocations, and short

fatigue crack of near-threshold stage normally propagated along the favoured slip plane within a grain in many metallic materials. Crystallographic orientation change across a grain boundary could result in crack-plane tilt and twist, slip-band blocked by the grain boundary, and then reduce the effective driving force for crack growth. It is believed that finer grain structure introduced more grain boundaries, and reinforced this effect, thereby improving the microcrack propagation resistance.

There are coarse black particles in Fig. 6, these particles are known to be intermetallic phases. The EDS analysis (Table 3) exhibits two different kinds of Cu containing particles: one containing Al, Cu and Fe, which is believed to be $\text{Al}_7\text{Cu}_2\text{Fe}$; the other containing Al, Cu and Mg, which is identified as S phases (Al_2CuMg) [24,25]. These particles are residual phases that did not dissolve in the matrix during the solution treatment. These phases have higher hardness than the matrix, and hence, they may induce additional strain localization and thus degrade the fatigue properties.

Table 3 Chemical compositions of areas in Fig. 6 of aged Al–Zn–Mg–Cu–Zr–(Sn) alloys obtained by EDS analysis

Phase code	$x(\text{Al})/\%$	$x(\text{Cu})/\%$	$x(\text{Fe})/\%$	$x(\text{Mg})/\%$
A	69.36	15.52	–	15.12
B	78.45	14.45	7.01	–
C	66.20	16.21	–	17.58
D	74.75	17.01	8.24	–

The bright-field TEM micrographs of the double-aged alloys are shown in Fig. 7. It is well known that with increasing aging temperature, the precipitates in a 7050 aluminum alloy may be Guinier–Preston (GP), η' , or η phases [26]. Fine plate-like and rod-like precipitates are distributed in the aluminum matrix. According to the selected-area electron diffraction (SAED) patterns, the plate-like precipitates are η' phase and the rod-like precipitates are η phase [27–31]. This indicates that after double aging, both the alloys are overaged. For overaged alloys, the precipitates within the grains are mainly η phases, which are incoherent with the matrix and coarse. These coarser phases within the grains may promote void formation due to continued plastic flow around them, and these microvoids may contribute to fatigue crack growth [32,33]. Comparison of Fig. 7(a) with 7(b) reveals that the η phase in the Sn-containing alloy is finer and more disperse than that in the Sn-free alloy. Thus, the overaged Al–Zn–Mg–Cu–Zr–Sn alloy shows a relatively high resistance to fatigue crack propagation. The finer grain size in the aged Sn-containing alloy should contribute at least partly to a finer and more disperse precipitate. It has been reported that a fine-grained microstructure can accelerate the precipitation of a new phase, thereby making the precipitated phase more disperse [34,35]. Alternatively, this may suggest that the addition of Sn to the Al–Zn–Mg–Cu alloy could slow down the coarsening of the precipitates during aging.

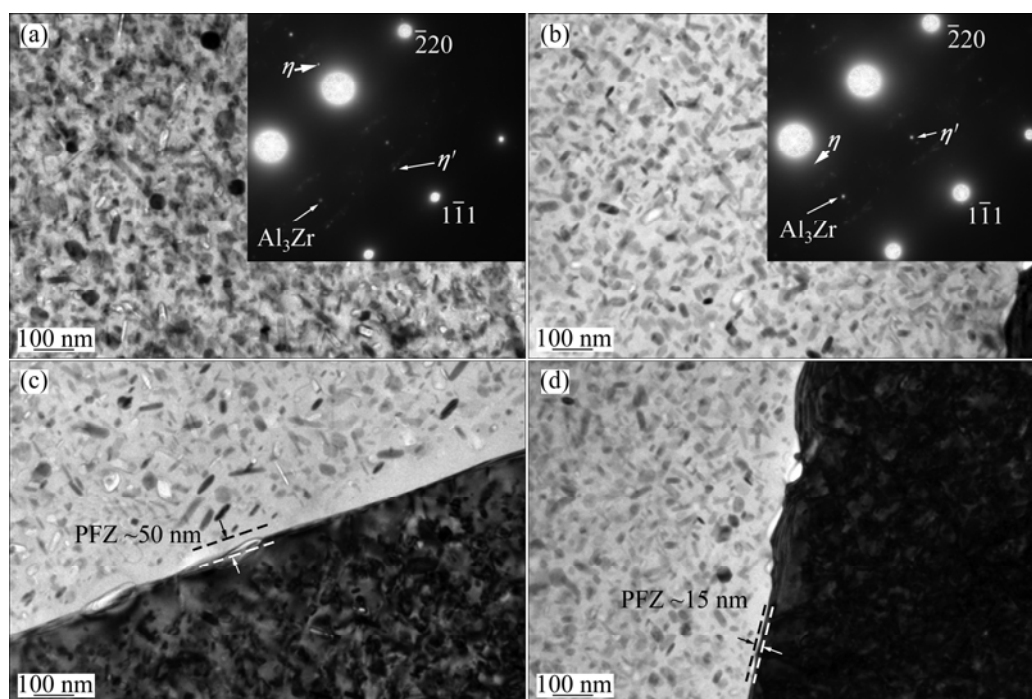


Fig. 7 TEM images of alloys in $\langle 112 \rangle_{\text{Al}}$ direction and corresponding selected-area electron diffraction (SAED) patterns after double-aging treatment: (a), (c) Al–Zn–Mg–Cu–Zr; (b), (d) Al–Zn–Mg–Cu–Zr–Sn

It is generally accepted that the precipitate-free zone (PFZ) adjacent to the grain boundary affects the rate of fatigue crack growth. Because the strength of the matrix is higher than that of the PFZ, there is additional strain localization, which triggers grain boundary failure [36]. As shown in Figs. 7(c) and (d), the width of the PFZ of the Sn-containing alloy is less than one-half that of the alloy without Sn. Thus, the Al–Zn–Mg–Cu–Zr–Sn alloy exhibits a lower rate of fatigue crack growth.

Furthermore, the precipitates at the grain boundaries also influence the rate of fatigue crack growth [5]. LUDTKA and LAUGHLIN [37] suggested that grain boundary cracking is initiated by the formation of voids at the coarse precipitates at the grain boundaries and that these voids subsequently coalesce and extend along the grain boundary. The more the precipitates at the grain boundaries are, the greater the probability of void formation around the coarse grain boundary particles and crack propagation is [38,39]. As shown in Figs. 7(c) and (d), the grain boundary particles are smaller in the Sn-containing alloy, and therefore, there is less damage caused by grain boundary cracking [40].

Figure 8 shows the backscattered electron (BSE) image of aged Al–Zn–Mg–Cu–Zr–Sn alloy and the element mapping of Mg and Sn. It should be noted that a new phase, Mg–Sn, is present in the aged Al–Zn–Mg–Cu–Zr–Sn alloy. EDS analysis (Table 4) reveals that the Mg to Sn ratio in this phase is close to 2:1. The new phase in the aged Sn-containing alloy is believed to be the Mg_2Sn phase, based on the XRD results in Fig. 9. Because the solubility of Sn in Al is less than 0.1%, it is thought that most of the Mg_2Sn , even if not all of it, was not involved in the solution and aging process. It is clear that the distribution of Mg and Sn is random (Fig. 8). This implies that Sn dissolved in the Al matrix may contribute to strength improvement as well as to the appearance of finer precipitates during aging.

Table 4 Chemical compositions of Mg–Sn phase obtained by EDS analysis

$x(Al)/\%$	$x(Mg)/\%$	$x(Sn)/\%$
75.43	16.44	8.13

The Mg_2Sn phase regions are larger than 1 μm . Because this phase is formed mainly during solidification and is distributed at the grain boundary, it has a negative impact on the fatigue performance. Nevertheless, the addition of Sn produces a finer aged microstructure, smaller precipitates, and a narrower PFZ, all of which probably have a significant impact on fatigue performance.

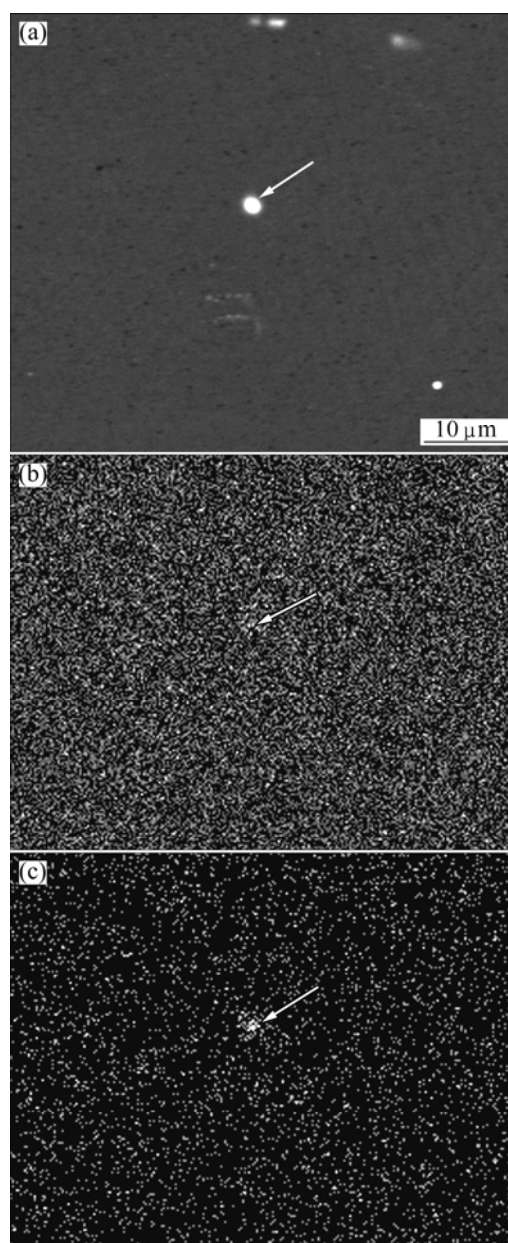


Fig. 8 BSE image of double-aged Al–Zn–Mg–Cu–Zr–Sn alloy (a) and element mapping of Mg (b) and Sn (c)

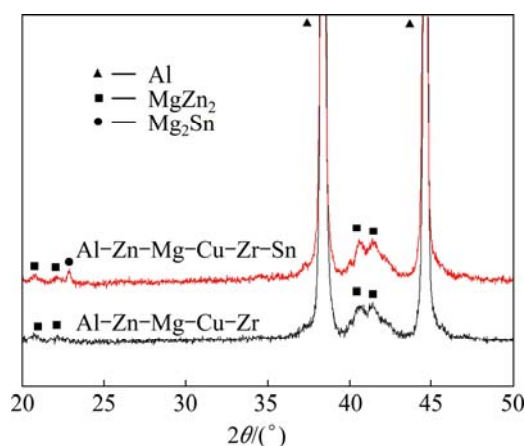


Fig. 9 XRD patterns of aged alloy plates

5 Conclusions

1) After the addition of Sn, growth of the recrystallization grains in the solution-treated Al–Zn–Mg–Cu–Zr alloy is obstructed and the grain size is refined, resulting in improved tensile properties.

2) In the overaged Al–Zn–Mg–Cu–Zr–Sn alloy, the η phases are finer and more disperse than these in the Sn-free alloy. These finer phases may reduce void formation during continued plastic flow, and contribute to the high FCP resistance.

3) The PFZ becomes narrow (and even disappears), and the grain boundary precipitates are smaller in the Sn-containing alloy, both of which reduce the damage caused by grain boundary cracking.

References

- [1] JIAN Hai-gen, JIANG Feng, WEN Kang, JIANG Long, HUANG Hong-feng, WEI Li-li. Fatigue fracture of high-strength Al–Zn–Mg–Cu alloy [J]. Transactions of Nonferrous Metals Society of China, 2009, 19: 1031–1036.
- [2] WANG Hui, LUO Ying-bing, FRIEDMAN P, CHEN Ming-he, GAO Lin. Warm forming behavior of high strength aluminum alloy AA7075 [J]. Transactions of Nonferrous Metals Society of China, 2012, 22: 1–7.
- [3] SENKOV O N, SENKOVA S V, SHAGIEV M R. Effect of Sc on aging kinetics in a direct chill cast Al–Zn–Mg–Cu alloy [J]. Metallurgical and Materials Transactions A, 2008, 39: 1034–1053.
- [4] BAI S, LIU Z Y, LI Y T, HOU Y H, CHEN X. Microstructures and fatigue fracture behavior of an Al–Cu–Mg–Ag alloy with addition of rare earth Er [J]. Materials Science and Engineering A, 2010, 527: 1806–1814.
- [5] ZHANG Zhuo, CHEN Kang-hua, FANG Hua-chan, QI Xiong-wei, LIU Gang. Effect of Yb addition on strength and fracture toughness of Al–Zn–Mg–Cu–Zr aluminum alloy [J]. Transactions of Nonferrous Metals Society of China, 2008, 18: 1037–1042.
- [6] MONDOLFO L F. Aluminum alloys: Structure and properties [M]. London: Butterworths, 1976.
- [7] RINGER S P, HONO K, SAKURAI T. The effect of trace additions of Sn on precipitation in Al–Cu alloys: An atom probe field ion microscopy study [J]. Metallurgical and Materials Transactions A, 1995, 26: 2207–2217.
- [8] SILCOCK J M, FLOWER H M. Comments on a comparison of early and recent work on the effect of trace additions of Cd, In, or Sn on nucleation and growth of θ' in Al–Cu alloys [J]. Scripta Materialia, 2002, 46: 389–394.
- [9] BANERJEE S, ROBI P S, SRINIVASAN A, LAKAVATH P K. Effect of trace additions of Sn on microstructure and mechanical properties of Al–Cu–Mg alloys [J]. Materials & Design, 2010, 31: 4007–4015.
- [10] MOHAMED A M A, SAMUEL F H, SAMUEL A M, DOTY H W, VALTIERRA S. Influence of Tin addition on the microstructure and mechanical properties of Al–Si–Cu–Mg and Al–Si–Mg casting alloys [J]. Metallurgical and Materials Transactions A, 2008, 39: 491–501.
- [11] ASTM E 647–08. Standard test method for measurement of fatigue crack growth rates [S].
- [12] LYNCH S P, TREVENA P. Stress corrosion cracking and liquid metal embrittlement in pure magnesium [J]. Corrosion, 1998, 44: 113–124.
- [13] SRIVATSAN T S, KOLAR D, MAGNUSEN P. The cyclic fatigue and final fracture behavior of aluminum alloy 2524 [J]. Materials & Design, 2002, 23: 129–139.
- [14] SHAN D, HASHEMI H N. Fatigue-life prediction of SiC particulate reinforced aluminum alloy 6061 matrix composite using AE stress delay concept [J]. Journal of Materials Science, 1999, 34: 3263–3273.
- [15] BRAUN R. Transgranular environment-induced cracking of 7050 aluminium alloy under cyclic loading conditions at low frequencies [J]. International Journal of Fatigue, 2008, 30: 1827–1837.
- [16] SHAMA V M J, KUMAR K S, RAO B N, PATHAK S D. Effect of microstructure and strength on the fracture behavior of AA2219 alloy [J]. Materials Science and Engineering A, 2009, 502: 45–53.
- [17] DU Z W, SUN Z M, SHAO B L, ZHOU T T, CHEN C Q. Quantitative evaluation of precipitates in an Al–Zn–Mg–Cu alloy after isothermal aging [J]. Materials Characterization, 2006, 56: 121–128.
- [18] SHA G, CERESO A. Kinetic monte carlo simulation of clustering in an Al–Zn–Mg–Cu alloy (7050) [J]. Acta Materialia, 2005, 53: 907–917.
- [19] MORRIS W L. Microcrack closure phenomena for Al2219-T851 [J]. Metallurgical Transactions A, 1979, 10: 5–11.
- [20] MORRIS W L. The noncontinuum crack tip deformation behavior of surface microcracks [J]. Metallurgical Transactions A, 1980, 11: 1117–1123.
- [21] ZHAI T, WILKINSON A J, MARTIN J W. A crystallographic mechanism for fatigue crack propagation through grain boundaries [J]. Acta Materialia, 2000, 48: 4917–4927.
- [22] BRUZZI M S, MCHUGH P E. Micromechanical investigation of the fatigue crack growth behaviour of Al–SiC MMCs [J]. International Journal of Fatigue, 2004, 26: 795–804.
- [23] BILBY B A, COTTERLL A H, SWINDEN K H. The spread of plastic yield from a notch [J]. Proceedings of the Royal Society A, 1963, 272: 304–314.
- [24] KAMP N, SINCLAIR I, STARINK M J. Toughness—strength relations in the overaged 7449 Al-based alloy [J]. Metallurgical and Materials Transactions A, 2002, 33: 1125–1136.
- [25] LI Jun-peng, SHEN Jian, YAN Xiao-dong, MAO Bai-ping, YAN Liang-ming. Microstructure evolution of 7050 aluminum alloy during hot deformation [J]. Transactions of Nonferrous Metals Society of China, 2010, 20: 189–194.
- [26] BERG L K, GJONNES J, HANSEN V, LI X Z, WEDEL M K, WATERLOO G, SCHRYVERS D, WALLEMBERG L R. GP-zones in Al–Zn–Mg alloys and their role in artificial aging [J]. Acta Materialia, 2001, 49: 3443–3451.
- [27] SHA G, CERESO A. Early-stage precipitation in an Al–Zn–Mg–Cu alloy (7050) [J]. Acta Materialia, 2004, 52: 4503–4516.
- [28] SONG M, CHEN K H. Effects of the enhanced heat treatment on the mechanical properties and stress corrosion behavior of an Al–Zn–Mg alloy [J]. Journal of Materials Science, 2008, 43: 5265–5273.
- [29] CHEN J Z, ZHEN L, YANG S J, SHAO W Z, DAI S L. Investigation of precipitation behavior and related hardening in AA7055 aluminum alloy [J]. Materials Science and Engineering A, 2009, 500: 34–42.
- [30] NING Z L, GUO S, CAO F Y, WANG G J, LI Z C, SUN J F. Microstructural evolution during extrusion and ECAP of a spray-deposited Al–Zn–Mg–Cu–Sc–Zr alloy [J]. Journal of Materials Science, 2010, 45: 3023–3029.
- [31] LIU Sheng-dan, ZHANG Yong, LIU Wen-jun, DENG Yun-lai, ZHANG Xin-ming. Effect of step-quenching on microstructure of aluminum alloy 7055 [J]. Transactions of Nonferrous Metals Society of China, 2010, 20: 1–6.

- [32] HORNBOKEN E, GAHR K H Z. Microstructure and fatigue crack growth in a γ -Fe-Ni-Al alloy [J]. Acta Metallurgica, 1976, 24: 581–592.
- [33] DESMUKHA M N, PANDEY R K, MUKHOPADHYAY A K. Effect of aging treatments on the kinetics of fatigue crack growth in 7010 aluminum alloy [J]. Materials Science and Engineering A, 2006, 435–436: 318–326.
- [34] DUMONT M, LEFEBVRE W, COTTIGNIES B D, DESCHAMPS A. Characterisation of the composition and volume fraction of η' and η precipitates in an Al-Zn-Mg alloy by a combination of atom probe, small-angle X-ray scattering and transmission electron microscopy [J]. Acta Materialia, 2005, 53: 2881–2892.
- [35] LIU H S, QIAO X, CHEN Z H, JIANG R P, LI X Q. Effect of ultrasonic vibration during casting on microstructures and properties of 7050 aluminum alloy [J]. Journal of Materials Science, 2011, 46: 3923–3927.
- [36] WANG M H, WANG W H, ZHOU J, DONG X G, JIA Y J. Strain effects on microstructure behavior of 7050-H112 aluminum alloy during hot compression [J]. Journal of Materials Science, 2012, 47: 3131–3139.
- [37] LUDTKA G M, LAUGHLIN D E. The effect of solute content on the slip behavior in 7xxx series aluminum alloys [J]. Metallurgical and Materials Transactions A, 1981, 12: 2083–2091.
- [38] VASUDEVAN A K, DOHERTY R D. Grain boundary ductile fracture in precipitation hardened aluminum alloys [J]. Acta Metallurgica, 1987, 35: 1193–1219.
- [39] KIMAN I. The relation between microstructure and toughness in 7075 aluminum alloy [J]. Metallurgical Transactions, 1971, 2: 1761–1771.
- [40] XUE Y, KADIRI H E, HORSTEMYER M F, JORDON J B, WEILAND H. Micromechanisms of multistage fatigue crack growth in a high-strength aluminum alloy [J]. Acta Materialia, 2007, 55: 1975–1984.

Al-Zn-Mg-Cu-Zr(-Sn)合金的 强度和疲劳断裂行为

陈璐¹, 严安¹, 刘华山¹, 李晓谦²

1. 中南大学 材料科学与工程学院, 长沙 410083;

2. 中南大学 机电工程学院, 长沙 410083

摘要: 通过拉伸试验和疲劳裂纹扩展试验研究了 Al-Zn-Mg-Cu-Zr(-Sn)合金的强度和疲劳断裂行为。运用光学显微镜(OM)、扫描电镜(SEM)和透射电子显微镜(TEM)对试验合金的微观组织进行分析检测。结果表明, Sn 的添加可以阻碍固溶时 Al-Zn-Mg-Cu-Zr 合金晶粒的长大,也使得过时效 Al-Zn-Mg-Cu-Zr-Sn 合金的晶界无沉淀析出带(PFZ)变窄及晶界析出相变小,因此,提高了合金的抗疲劳裂纹扩展能力。此外,过时效的 Al-Zn-Mg-Cu-Zr-Sn 合金具有较高的抗拉强度。

关键词: Al-Zn-Mg-Cu-Zr; Sn; 强度; 疲劳断裂行为; 微观组织

(Edited by Hua YANG)